Pressure/Temperature and Reaction Phase Diagram for Dinitro Azetidinium Dinitramide

T. P. Russell*

Chemistry Division, Code 6110, Naval Research Laboratory, Washington, D.C. 20375

G. J. Piermarini

Materials Science and Engineering Laboratory, National Institute of Standards and Technology, Gaithersburg, Maryland 20899

P. J. Miller

Naval Surface Warefare Center, Silver Spring, Maryland 20901

Received: September 12, 1996[⊗]

The pressure/temperature and reaction phase diagram for dinitro azetidinium dinitramide (DNAZ-DN) has been delineated using a high-pressure diamond anvil cell with Fourier transform infrared spectroscopy (FTIR), Raman spectroscopy, and optical polarizing light microscopy. The phase diagram was determined between ambient pressure and 10.0 GPa over the temperature range from −75 °C to decomposition temperatures or >150 °C. The phase diagram delineates the melt curve for α-DNAZ-DN, a reversible phase transformation in α-DNAZ-DN forming a new high-pressure polymorph, β-DNAZ-DN, and also identifies the pressure and temperature conditions for solid state decomposition of β-DNAZ-DN. FTIR and Raman spectra were obtained for both the α and β phases as a function of pressure at room temperature. The new high-pressure β polymorph could not be retrieved to ambient conditions.

Introduction

Recently, the synthesis of a stabilized dinitramide anion was discovered that could be associated with both inorganic and organic cations to provide a new class of energetic salt materials.[1] These compounds are potential replacements for ammonium nitrate or ammonium perchlorate in propellant and explosive applications. The current emphasis has been on the synthesis, thermal decomposition, and structural determination of the newly synthesized dinitramide salt compounds.[1−9] Some work has emphasized the structural changes and effects of extreme conditions on some dinitramide salt compounds.[7,8] One organic dinitramide salt that is a potential candidate as an explosive and minimum smoke propellant ingredient is dinitro azetidinium dinitramide (DNAZ-DN). Some physical and chemical properties of dinitro azetidinium salts, including DNAZ-DN, have recently been reported.[9] DNAZ-DN melt/decomposition at 136 °C was reported at ambient pressure.[9]

The crystal structure of α-DNAZ-DN has been determined.[10] α-DNAZ-DN is orthorhombic with *Cm*21 symmetry and a density of 1.791 g/cm^3.[10] A model diagram for DNAZ-DN showing the arrangement of the atoms constituting one molecular unit is shown in Figure 1. The molecule of DNAZ-DN (6H, 3C, 6N, 8O) consists of an azetidine ring with two NO_2 groups appended to the ring carbon opposite the protonated ring amine forming the organic cation and an associated dinitramide anion. As far as we know, no polymorphs of DNAZ-DN have been reported. In this paper, we report the discovery of a reversible phase transition in α-DNAZ-DN forming a new high-pressure polymorph, β-DNAZ-DN. The transition was determined by optical polarizing light microscopy (OPLM), Fourier transform infrared spectroscopy (FTIR), and Raman spectroscopy. Infrared and Raman spectra were obtained for both the α-DNAZ-DN and β-DNAZ-DN polymorphs. The decomposition parameters as a function of temperature and pressure are also presented. An estimated pressure/temperature and reaction phase diagram for DNAZ-DN is described.

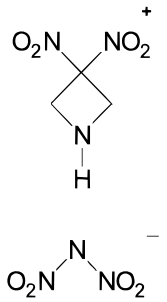

Figure 1. Model diagram of DNAZ-DN showing the arrangement of the atoms constituting one molecular unit. Note that two NO_2 groups are appended to a single ring carbon of the azetidine ring and the dinitramide anion is associated with the protonated amine.

Experimental Procedures

The experimental techniques employed in the present work were reported in detail earlier.[11−18] Thus, only a brief description is given here for the sake of clarity. The diamond anvil cell (DAC) used in this work is fabricated from a high-temperature, high-strength superalloy, Inconel 718, and is designed for 180° transmission and reflection measurements with sustained static temperatures between −125 and 600 °C.[11] It is based on the original NBS DAC cell design.[18] The diamond anvil piston assembly is surrounded by a removable miniature resistance coil heater with high-power output (∼70 Ω resistance).[11] The heater coil is bifilar and is sheathed in Inconel 600 alloy packed with MgO powder for electrical insulation. A thyristor controller and a silicon-controlled rectifier (SCR) control the power input to the heater. Automatic control of the heating rate is accomplished with proportional, integral, and derivative features. Other features include time-proportional

* Corresponding author.
[⊗] Abstract published in *Advance ACS Abstracts,* April 1, 1997.

S1089-5647(96)02826-X

heating, temperature overshoot inhibition, and direct temperature readout. This system permits routine static heating of the sample in a DAC. The temperature is measured by a chromel-alumel thermocouple with its bead in contact with an Inconel X750 alloy gasket, which confines the sample under pressure. The sample temperature can be set and automatically maintained to ±1 °C with an estimated accuracy of ±3 °C at 300 °C. The sample temperature was calibrated using a fixed-point calibration method based on the melting point of pure materials.[11] Pressures are measured by the ruby fluorescence technique and are accurate to ±0.05 GPa when measurements are made in a hydrostatic environment and room temperature.[11,12] At elevated temperatures both line broadening and decrease in fluorescence intensity contribute to an increase in the pressure measurement uncertainty, which is approximately 0.1 GPa at 300 °C. These effects increase the uncertainty of λ, the wavelength of the R_1 line, and the temperature correction to λ, which shifts with temperature (temperature shifts in λ are in the same direction as the pressure shift). A temperature correction for λ has been determined from ruby fluorescence measurements made at 1 atm in the DAC and are included in our overall uncertainty. Uncertainty in the pressure measurement is even larger, 0.15 GPa when NaCl is employed for spectroscopic measurements due to the absence of strictly hydrostatic conditions. The DAC can be mounted on a micrometer positioning device for optical polarizing light microscopy, ruby fluorescence pressure measurements, Fourier transform infrared spectroscopy, and Raman spectroscopy measurements, as described below.

Optical Polarizing Light Microscopy and Ruby Fluorescence Measurements. Our ruby fluorescence pressure measurement system, which is also used for optical polarizing microscopy studies, has been described in detail earlier.[13] The DAC is positioned onto the optic axis of the microscope with the ruby or sample in focus. This technique was employed for ruby fluorescence measurements and also for polarized light microscopy experiments to study high-temperature/high-pressure phase transitions (birefringence measurements). The ruby R_1 line excitation (fluorescence) is accomplished with an Ar ion laser (514.5 nm) operating at a maximum continuous wave power of 15 mW. The focused laser beam is approximately 10−15 μm in diameter, which is roughly the size of the ruby sphere.

The transitions were determined by birefringence measurements on single crystals of DNAZ-DN using one of two pressure-transmitting media, e.g., liquid N_2 and *n*-pentane/isopentane (1:1 by volume) under polarizing light. *n*-Pentane/isopentane (1:1 by volume) is a hydrostatic pressure transmitting medium up to 6.0 GPa,[13] and liquid N_2[19] is hydrostatic up to 37.4 GPa. Both mediums provide a sharp image of the single crystals with clearly discernible changes in birefringence such as a dramatic change in color progressing as a wave across the crystal face. FTIR and Raman measurements on thin sheets of DNAZ-DN were accomplished in NaCl, as a quasi-hydrostatic pressure transmitting medium, and N_2(1). Transitions are also observed in thin sheets prepared for spectroscopic studies, but these effects are less dramatic and sometimes are not even detected by optical polarizing light microscopy.

Fourier Transform Infrared Spectroscopy and Raman Microscopy. Infrared absorption spectra are recorded on a Nicolet FTIR spectrometer, employing an MCT-A (narrow band) detector for improved sensitivity. As in earlier work, the sample is prepared as a thin sheet (5−10 μm thick) in a gasketed DAC containing either NaCl compacted to transparency or N_2(1). Both NaCl and N_2(1) provide both a visible and infrared window approximately 250 μm in diameter.[9,16]

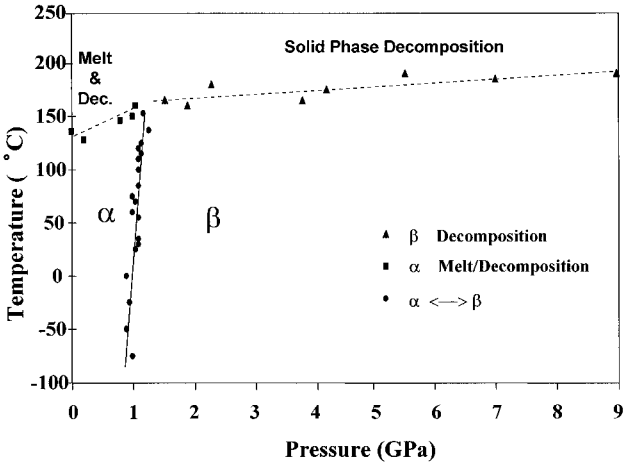

Figure 2. Pressure/temperature reaction/phase diagram for DNAZ-DN showing the general features of phase stability for the two polymorphs (α and β) as well as the thermal decomposition regions for the α and β phases.

Embedded in the medium is a small ruby sphere that serves as the pressure sensor. FTIR spectra were collected at all pressure and temperature conditions studied.

Micro-Raman spectra are recorded using a SPEX 1877A triple monochromator and a Photometrics liquid nitrogen cooled CCD detector for improved sensitivity. A Spectra Physics Ar ion laser operating at 514.5 nm and a power of 55 mW at the sample was employed. Raman spectra are collected on the samples prepared as a thin film in N_2(1). Both infrared and Raman spectra were collected on a single sample at the same pressure and temperature conditions on the sample.

Results and Discussion

The DNAZ-DN pressure/temperature and reaction phase diagram is presented initially to introduce the reader to the general features determined in this work. A complete description of the experimental results used to support the proposed phase diagram is presented in the following paragraphs.

Our complete pressure/temperature and reaction phase diagram for DNAZ-DN is presented in Figure 2. The general features of the phase diagram are the delineation of the stability fields of two polymorphs (α and β) and the liquidus material. In addition, the pressure and temperature reaction regimes for liquidus DNAZ-DN and β-DNAZ-DN are presented. The diagram is termed pressure/temperature and reaction phase diagram because the diagram provides both equilibrium as well as chemical reaction processes as a function of pressure and temperature.

The polymorphs' stability fields we have determined are as follows: (1) the orthorhombic phase, α, is stable between atmospheric pressure and 1.05 ± 0.05 GPa from −75 to 136 °C; (2) the liquidus phase stable from atmospheric pressure to 1.0 GPa between 136 to 146 °C; (3) the high-pressure polymorph, β, stable above 1.0 GPa between −50 °C and decomposition temperatures. The equilibrium phase boundaries shown in Figure 2 are designated by solid lines, while the unidirectional transition boundaries are designated by dashed lines. On the basis of our results, we think the phase boundaries shown delineate the thermodynamic stability fields of the pure material. The thermal decomposition pressure and temperature parameters have also been determined and reflect relatively rapid decomposition within 2−3 min. Slow decomposition is observed at lower temperatures after extended periods of sample heating at a constant temperature.

Prior to this effort no other structures were known for DNAZ-DN. Therefore, the initial material investigated was α-DNAZ-DN. Between −75 and 136 °C at atmospheric pressure, no phase transitions were observed in α-DNAZ-DN. Under microscopic polarized light, α-DNAZ-DN melting was observed at 136 °C and ambient pressure. A color wave progressing through the material immediately followed by a change in opacity was detected. Therefore, it is believed melting occurs prior to decomposition. Due to the immediate decomposition of the material, an accurate measurement of the equilibrium liquid/solid phase boundary could not be determined. However, an estimate of the solid/liquid boundary was accomplished. Each data point on the solid/liquid boundary was determined with a fresh α-DNAZ-DN sample pressed to the desired starting pressure and heated. Sample pressures were measured as a function of temperature during heating. The sample was heated at 2 °C/min until melt/decomposition was observed. A linear least squares fit to the observed data was applied to delineate the temperature/pressure dependency of the solid/liquid boundary from atmospheric pressure to 1.0 GPa between 136 and 145 °C. Uncertainty in the delineated solid/liquid boundary may be due to several factors. First, the transition is only observed unidirectionally, i.e., as the temperature is increased using a 2 °C/min heating rate. Second, because of the experimental error in pressure measurement, a 0.05 GPa pressure increase may occur under the reported temperature/pressure conditions. This would result in raising the observed sample melting temperature. Finally, liquid DNAZ-DN begins to decompose immediately. Although some error is associated with the measurements, the observed data provide an estimate of the solid/liquid phase boundary, represented as a dashed line in Figure 2. Below 1.0 GPa, no other chemical and/or physical changes were observed in α-DNAZ-DN.

Under continued microscopic examination of α-DNAZ-DN with polarized light, a birefringence change was observed in single crystals between 1.0 and 1.1 GPa. The pressure was increased slowly at 0.05 GPa intervals (at a constant temperature), and the crystal was studied for 3−5 min before the next pressure increase. The birefringence effect was observed to be reversible and very rapid once initiated. A color wave progressing rapidly through the crystal was detected. The crystal was observed to jump in the transmitting medium during the color wave progression. The progressing color wave through the crystal is only detected at pressures around 1.1 GPa when the pressure is increased as described above. When pressure increases greater than 0.1−0.2 GPa were employed, the transition was detected at pressures as high as 2.2 GPa. The progressing wave was not observed under these conditions. However, a change in birefringence and movement of the crystal was detected. When lowering the pressure slowly at 0.05 GPa intervals and waiting 3−5 min before the next pressure decrease, the reverse transition is observed at 1.0 GPa. A birefringence change coinciding with crystal movement was observed. The reverse transition pressure was detected at pressures as low as 0.7 GPa when the pressure increments were greater than 0.1−0.2 GPa increments. No cracking of the crystal is observed even after multiple oscillations through the reversible transition. Similar results are observed at all temperatures (−75 to 140 °C) during pressure oscillation around the transition boundary.

FTIR and Raman spectra of DNAZ-DN were collected as a function of pressure at room temperature as a thin film in a hydrostatic medium of N_2(1) to identify the polymorphic structures associated with transformation described above. Figures 3 and 4 show the three infrared and Raman spectra (respectively) that were collected at different pressures bracketing the transition at room temperature. The infrared and Raman frequencies for the α- and β-DNAZ-DN polymorphs are listed in Table 1. Tentative assignments for the observed vibrational frequencies are also given. Spectrum A (Figures 3 and 4) is the spectrum of α-DNAZ-DN at 0.6 GPa. Spectrum B (Figures 3 and 4) is the collected spectrum for β-DNAZ-DN when the pressure has been increased from 0.6 to 1.2 GPa. Spectrum C (Figures 3 and 4) was collected after lowering the pressure from 1.2 to 0.9 GPa. The resulting spectrum shows the reverse transformation to α-DNAZ-DN. Therefore, a reversible solid/solid phase transition between α ↔ β DNAZ-DN is detected between 1.0 and 1.1 GPa. A uniform shift in the vibrational frequencies of DNAZ-DN was observed up to 1.0 GPa. At 1.1 GPa, a negative or discontinuous shift in the vibrational frequencies of DNAZ-DN was detected. In addition, several new infrared and Raman frequencies were observed (Table 1). This indicates a first-order phase transition in α-DNAZ-DN at 1.1 GPa, forming a new high-pressure polymorph, β-DNAZ-DN. A continuous shift in the vibrational frequencies of

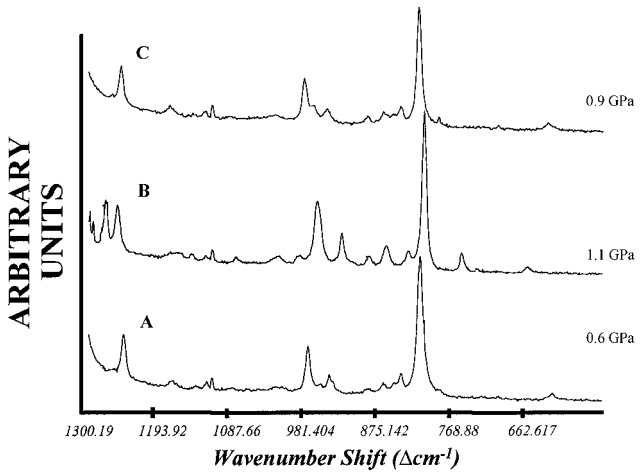

Figure 3. Three infrared absorption spectra of DNAZ-DN (A, B, and C) at room temperature and the following pressures: (A) for α-DNAZ-DN at 0.6 GPa; (B) for β-DNAZ-DN after the pressure had been increased above the α ↔ β transition to 1.1 GPa; and (C) for α-DNAZ-DN, after lowering the pressure from 1.1 GPa to 0.9 GPa. The return to α-DNAZ-DN (C) after pressure cycling demonstrates the reversibility of the α ↔ β transformation.

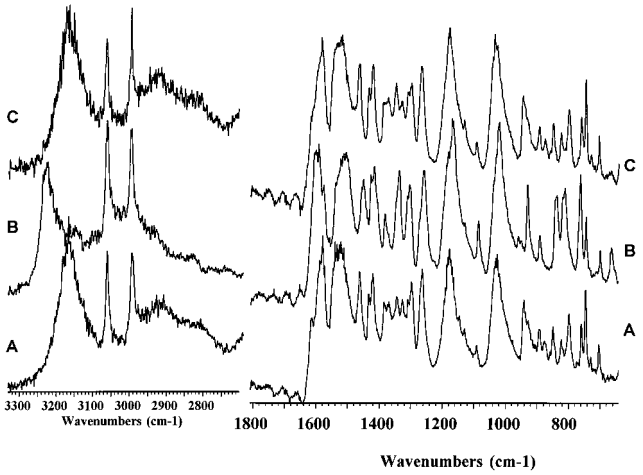

Figure 4. Three Raman spectra of DNAZ-DN (A, B, and C) at room temperature and the following pressures: (A) for α-DNAZ-DN at 0.6 GPa; (B) for β-DNAZ-DN after the pressure had been increased above the α ↔ β transition to 1.1 GPa; and (C) for α-DNAZ-DN, after lowering the pressure from 1.1 GPa to 0.9 GPa. The return to α-DNAZ-DN (C) after pressure cycling demonstrates the reversibility of the α ↔ β transformation.

TABLE 1: Mid-IR Frequencies (7550−1800 and 2500−4000) and Raman Frequencies (500−4000) for the α-DNAZ-DN at Room Temperature and 0.9 GPa and *β*-DNAZ-DN at Room Temperature and 1.1 GPa; Tentative Assignments for the Observed Vibration Frequencies Are Provided[a]

observed vibrational frequencies for α-DNAZ-DN at 0.9 GPa			observed vibrational frequencies for *β*-DNAZ-DN at 1.1 GPa			tentative assignments
3229	b,str	IR				$\nu(CH_2)$ sym/asym
3155	b,wk	IR	3165	b,vstr	IR	ν(CH) sym/asym
3066	sh,vstr	IR	3062	s,vstr	IR	ν(N−H) sym/asym
3003	sh,vstr	IR	2998	s,vstr	IR	
1603	b,vs	IR	1607	s,vstr	IR	
1593	b,vs	IR	1582	b,vstr	IR	$\nu(NO_2)$ and $\nu(N-(NO_2)_2)$
1577	b,vstr	IR				
1514			1529			$\nu(N-NH_2^+)$
1457	sh,str	IR	1464	s,str	IR	
1451	s,str	IR				
1428	s,str	IR	1435	str	IR	
1417	s,str	IR	1421			
1383	s,str	IR	1386	str	IR	
			1375			
1372	sh,str	IR	1371	str	IR	$\nu(NO_2)$ and $\delta(CH_2)$
1338		IR	1347	s,str	IR	
			1328	s,str	IR	
1313	s,str	IR	1311	sh,str	IR	
1306	s,vstr	IR	1299	s,vstr	IR	
			1275		Raman	
1260	s,str	IR	1267	s,vstr	IR	
1248		Raman	1258		Raman	ν(C−C) and ring vibrations
1180		Raman				
1169	s,str	IR	1182	s,vstr	IR	
			1174		Raman	
			1153		Raman	
1085	s,str	IR	1093	s,vstr	IR	ν(C−C) and ring vibrations
			1032	b,vstr	IR	
			1026		Raman	
1021	b,vstr	IR/Raman				
			995		Raman	
983		Raman				
960	s,wk	IR/Raman				
950	s,wk	IR/Raman				ν(C−N) stretch
931	s,str	IR	944	b,str	IR	
892	s,str	IR/Raman	896	s,str	IR/Raman	
874		Raman	879	b,str	IR/Raman	ν(C−C)
857		Raman	862	s,str	IR	
849		Raman	851	s,vstr	IR	$(N-NH_2^+)$ rocking vibration
844	sh,str	IR				
839	s,str	IR	838		Raman	
820	sh,str	IR/Raman	826	s,str	IR/Raman	ν(ONO) deformation
813	s,vstr	IR	802	s,str	IR	(CH) out-of-plane bending
763	s,vstr	IR	763	s,vstr	IR/Raman	
			749	s,vstr	IR	
745	s,str	IR	731	s,str	IR	
700	s,str	IR	707	s,str	IR	
665	s,str	IR	666		Raman	$\nu(NO_2)$ deformation
			640	s,str	IR	$\nu(NO_2)$ deformation
630		Raman				$\nu(NO_2)$ sym deformation

[a] s = sharp, b = broad, sh = shoulder, str = strong, vstr = very strong, sym = symmetric, asym = asymmetric.

β-DNAZ-DN was obtained at pressures up to 15.0 GPa. *β*-DNAZ-DN was not retrievable to ambient conditions.

The α/*β* transformation is identified to be reversible between −75 and 140 °C by OPLM, FTIR, and Raman spectroscopy. A linear least squares fit of the measured data points was performed to determine the phase boundary line for the α ↔ *β* transition over the temperature range indicated (Figure 2). The transition boundary is represented by a solid line. The delineated transition boundary is assumed to represent the equilibrium α ↔ *β* phase boundary. Hysteresis in the transformation is detected, but when the pressure was changed slowly (pressure intervals of 0.05 GPa every 3−5 min), the hysteresis is reduced to the experimental error of the ruby fluorescence pressure measurement technique. Therefore, the observed transformation is representative of near equilibrium conditions. Therefore, the solid line describes, in our opinion, an equilibrium condition between the α and *β* polymorphs of DNAZ-DN; that is, the transformation is reversible and can be approached from either phase.

Because of the transition hysteresis, the slope of the transition boundary was not readily evident from the data presented. The slope of the transition boundary was determined by FTIR spectroscopy. α-DNAZ-DN was pressurized to 0.9 GPa at 21 °C. The sample was initially heated 2 °C/min to 100 °C and held isothermally for 1−2 h at 0.9 GPa. No detectable changes in the IR absorption spectrum were observed. The sample was then cooled (2−5 °C/min) to −75 °C at 0.9 GPa. The sample temperature was held isothermally for 5−10 min at 10 deg intervals. At −50 °C, the α ↔ *β* transformation was observed. The transition was sluggish. Complete transformation required ∼1 h. Upon warming to −10 °C at 0.9 GPa, the reverse transformation was detected. The transformation was again

sluggish (~0.5−1 h for completion). α-DNAZ-DN was then pressurized to 1.2 GPa at 21 °C, forming β-DNAZ-DN. The sample was heated slowly at 5 deg intervals. The sample was held at a constant temperature for 10 min before the temperature was increased. At 90 °C and 1.2 GPa, the β → α transformation was observed. The transition rate was moderate (15−20 min for completion). Therefore, the α/β phase equilibrium phase boundary was determined to have a positive slope between −75 and 140 °C.

Between 1.1 and 10.0 GPa and −75 and 150 °C GPa, β-DNAZ-DN is the stable phase. No other chemical or physical changes in β-DNAZ-DN were observed in this pressure and temperature regime. β-DNAZ-DN decomposition was observed by OPLM and FTIR spectroscopy between 1.2 and 10.0 GPa above 150−175 °C. The decomposition temperature reported indicate a rapid decomposition rate (1−2 min for complete decomposition). Decomposition was determined by the disappearance of the infrared spectrum of the starting material. Optical polarizing light microscopy indicated no liquid formation prior to decomposition. Therefore, β-DNAZ-DN decomposes from the solid state. A linear least squares fit of the FTIR and OPLM decomposition data was performed to determine the temperature and pressure conditions for β-DNAZ-DN decomposition and is represented by a dashed line to indicate a high uncertainty in the exact pressure/temperature conditions. The uncertainty in the identified solid phase decomposition boundary may be due to several factors. One is the reaction was observed to be unidirectional. Another is the reported decomposition parameters describe a rapid rate of decomposition; that is, the sample is observed to decompose in 1−2 min.

Conclusions

The pressure/temperature and reaction phase diagram for DNAZ-DN has been determined up to 10.0 GPa between −75 and 175 °C. A high-pressure phase transition in α-DNAZ-DN was discovered and occurs at 1.05 ± 0.05 GPa, forming a new high-pressure polymorph, β-DNAZ-DN. The transformation is rapid and reversible and can be identified by a sharp birefringence change when single crystals are in a hydrostatic environment. Hysteresis is observed in the transition by rapid pressure application (0.1−0.2 GPa). The measured transition pressure was observed as high as 2.2 GPa or as low as 0.7 GPa. However when slowly pressurized (0.05 GPa every 3−5 min), the transition hysteresis may be reduced to the experimental error of the pressure measurement (±0.05 GPa). Under these conditions, the reversible transition was observed between 1.0 and 1.1 GPa. The transition was detected by discontinuous spectroscopic changes in the infrared and Raman spectra and by a birefringence change observed as a color wave progression through the crystal under optically polarized light. The presence of new infrared absorptions and Raman lines is also observed. The infrared and Raman spectra as a function of pressure indicate a uniform compression of α-DNAZ-DN up to the transition pressure and a uniform compression of β-DNAZ-DN up to 15.0 GPa. The new high-pressure phase (β-DNAZ-DN) was not retrievable to ambient pressure and temperature. The stability fields of the liquidus phase and two DNAZ-DN polymorphs (α and β) have been delineated as a function of temperature and pressure, permitting the determination of the equilibrium phase diagram for DNAZ-DN. The estimated stability fields for the two polymorphs (α and β) are as follows: (1) the stable monoclinic phase, α, stable between atmospheric pressure and 2.0 GPa and −75 and 136 °C and (2) a high-pressure polymorph, β, stable above 1.1 GPa between −75 °C and decomposition temperatures. In addition, the reaction chemistry of DNAZ-DN as a function of temperature and pressure was determined and included in the diagram. The temperature/pressure conditions for decomposition were determined as follows: liquidus DNAZ-DN decomposes between atmospheric pressure and 1.0 GPa at 136−146 °C; and β-DNAZ-DN polymorph decomposes between 1.0 and 10.0 GPa at 150−175 °C, via solid state decomposition.

Acknowledgment. The authors wish to acknowledge financial support from the Office of Naval Research and the Naval Surface Warfare Center Independent Research Program. Certain trade names and or products are mentioned in the text in order to adequately specify the experimental procedure and equipment used. In no case does such identification imply recommendation or endorsement by NIST or NRL nor does it imply that the product necessarily is the best available for the purpose.

References and Notes

(1) Bottaro, J. C.; Schmidt, R. J.; Renwell, P. E.; Ross, D. S. World Intellectual Property Organization, International Application Number PCT/US91/04268, December 26, 1991.

(2) Doyle, R. J. *Org. Mass Spectroscopy* **1993**, *28*, 83−91.

(3) Schmidt, R. J.; Krempp, M.; Bierbaum, V. M. *Int. J. Mass Spectrum. Ion Processes* **1992**, *117*, 621.

(4) Politzer, P.; Murrary, J. S.; Seminario, J. M.; Miller, R. *J. Mol. Struct.* **1992**, *262*, 155−170.

(5) Russell, T. P.; Stern, A. G.; Koppes, W. M.; Bedford, C. D. CPIA Publication, Proceedings of the JANAF Combustion Meeting, Hampton, VA, 19−23 October, 1992.

(6) Brill, T. B.; Brush, P. J.; Patil, D. G. *Combust. Flame* **1993**, *92*, (2), 178−186.

(7) Russell, T. P.; Miller, P. J.; Piermarini, G. J.; Block, S. Materials Research Society Symposium Proceedings, *Structure and Properties of Energetic Materials*; Liebenberg, D., Armstrong, R. W., Gilman, J. J., Eds.; Boston, MA, Nov 30−Dec 2, 1992, Vol 296.

(8) Russell, T. P.; Miller, P. J.; Piermarini, G. J.; Block, S. *J. Phys. Chem.* **1996**, *100* (8), 3248−3251.

(9) Hiskey, M. A.; Stinecipher, M. M.; Brown, J. E. *J. Energ. Mater.* **1993**, *11*, 157.

(10) Koppes, W.; Hiskey, M. A.; Gilardi, R. To be published, crystallography data is available upon request to R. Gilardi at Naval Research Laboratory).

(11) Barnett, J. D.; Block, S.; Piermarini, G. J. *Rev. Sci. Instrum.* **1973**, *44*, 1.

(12) Block, S.; Piermarini, G. J. *Phys. Today* **1976**, *29*, 44.

(13) Piermarini, G. J.; Block, S.; Barnett, J. D.; Forman, R. S. *J. Appl. Phys.* **1975**, *46*, 2774.

(14) Miller, P. J.; Piermarini, G. J.; Block, S. *Appl. Spectrosc.* **1984**, *38*, 680.

(15) Piermarini, G. J.; Block, S.; Miller, P. J. NATO Advanced Study Institute, *The Chemistry and Physics of Energetic Materials*; Bulusu, S., Ed.; Altavilla Milicia, Sicily, Sept 3−15, 1989, 1990, Vol. 309, pp 369−412.

(16) Miller, P. J.; Block, S.; Piermarini, G. J. *Combust. Flame* **1991**, *83*, 174.

(17) Piermarini, G. J.; Block, S.; Barnett, J. D. *J. Appl. Phys.* **1973**, *44*, 5377.

(18) Weir, C. E.; Lippincott, E. R.; Van Valkenberg, A.; Bunting, E. N. *J. Res. NBS* **1959**, *63A*, 55.

(19) Lesar, R.; Ekberg, S. A.; Jones, L. H.; Mills, R. A.; Schwalbe, L. A.; Schiferl, D. *Solid State Commun.* **1979**, *32*, 131−134.